Biochimica et Biophysica Acta 1847 (2015) 328–342

Contents lists available at ScienceDirect

Biochimica et Biophysica Acta

journal homepage: www.elsevier.com/locate/bbabio

Polyethylenimine architecture-dependent metabolic imprints and perturbation of cellular redox homeostasis

Arnaldur Hall [a,b,c,*], Ladan Parhamifar [a,b], Marina Krarup Lange [c], Kathrine Damm Meyle [d], May Sanderhoff [e], Helene Andersen [a,b], Martin Roursgaard [f], Anna Karina Larsen [a,b], Per Bo Jensen [e], Claus Christensen [c], Jiri Bartek [c,g], Seyed Moein Moghimi [a,b,*]

[a] Nanomedicine Research Group and Centre for Pharmaceutical Nanotechnology and Nanotoxicology, Department of Pharmacy, University of Copenhagen, Universitetsparken 2, DK-2100 Copenhagen Ø, Denmark
[b] NanoScience Centre, University of Copenhagen, Universitetsparken 5, DK-2100 Copenhagen Ø, Denmark
[c] Genome Integrity Unit, Danish Cancer Society Research Center, Copenhagen, Denmark
[d] Institute of Preventive Medicine, Bispebjerg and Frederiksberg Hospitals, The Capital Region, Copenhagen, Denmark
[e] Seahorse Bioscience Europa, Copenhagen, Denmark
[f] Section of Environmental Health, Department of Public Health, University of Copenhagen, DK-1014 Copenhagen K, Denmark
[g] Institute of Molecular and Translational Medicine, Faculty of Medicine and Dentistry, Palacky University, CZ-775 15 Olomouc, Czech Republic

ARTICLE INFO

Article history:
Received 14 August 2014
Received in revised form 17 November 2014
Accepted 3 December 2014
Available online 5 December 2014

Keywords:
Bioenergetics
Cell death
Glycolytic flux
Mitochondrial dysfunction
Oxidative stress
Polyethylenimine

ABSTRACT

Polyethylenimines (PEIs) are among the most efficient polycationic non-viral transfectants. PEI architecture and size not only modulate transfection efficiency, but also cytotoxicity. However, the underlying mechanisms of PEI-induced multifaceted cell damage and death are largely unknown. Here, we demonstrate that the central mechanisms of PEI architecture- and size-dependent perturbations of integrated cellular metabolomics involve destabilization of plasma membrane and mitochondrial membranes with consequences on mitochondrial oxidative phosphorylation (OXPHOS), glycolytic flux and redox homeostasis that ultimately modulate cell death. In comparison to linear PEI, the branched architectures induced greater plasma membrane destabilization and were more detrimental to glycolytic activity and OXPHOS capacity as well as being a more potent inhibitor of the cytochrome *c* oxidase. Accordingly, the branched architectures caused a greater lactate dehydrogenase (LDH) and ATP depletion, activated AMP kinase (AMPK) and disturbed redox homeostasis through diminished availability of nicotinamide adenine dinucleotide phosphate (NADPH), reduced antioxidant capacity of glutathione (GSH) and increased burden of reactive oxygen species (ROS). The differences in metabolic and redox imprints were further reflected in the transfection performance of the polycations, but co-treatment with the GSH precursor *N*-acetyl-cysteine (NAC) counteracted redox dysregulation and increased the number of viable transfected cells. Integrated biomembrane integrity and metabolomic analysis provides a rapid approach for mechanistic understanding of multifactorial polycation-mediated cytotoxicity, and could form the basis for combinatorial throughput platforms for improved design and selection of safer polymeric vectors.

Abbreviations: AMPK, AMP kinase; Anti-A, antimycin A; Asc, ascorbate; 2-DG, 2-deoxy-D-glucose; NAC, *N*-acetyl-cysteine; NaN_3, sodium azide; CI, complex I; CII, complex II; CIII, complex III; CIV, complex IV; CS, citrate synthase; cyt *c*, cytochrome *c*; DMEM, Dulbecco's Modified Eagle's Medium; ETS, electron transport system; ECAR, extracellular acidification rate; FBS, fetal bovine serum; FCCP, carbonyl cyanide 4-trifluoromethoxy phenylhydrazone; $FADH_2$, flavin adenine dinucleotide; GSH, reduced glutathione; GSSG, oxidized glutathione disulphide; IDH, isocitrate dehydrogenase; LDH, lactate dehydrogenase; ME, malic enzyme; Mna, malonic acid; MRR, maximum respiratory rate; NADH, nicotinamide adenine dinucleotide; NADPH, nicotinamide adenine dinucleotide phosphate; OCR, oxygen consumption rate; OXPHOS, oxidative phosphorylation; PBS, phosphate buffered saline; PMP, XF Plasma Membrane Permeabilizer; PPP, pentose phosphate pathway; PEI, polyethylenimine; RCR, respiratory control ratio; ROS, reactive oxygen species; Rote, rotenone; RPMI, Roswell Park Memorial Institute; TBHP, tert-butyl hydroperoxide; TCA cycle, tricarboxylic acid cycle; TMPD, *N,N,N′,N′*-tetramethyl-*p*-phenylenediamine.

* Corresponding authors at: DK-2100 Copenhagen Ø, Denmark.
E-mail addresses: arnaldur.hall@sund.ku.dk, ahall@cancer.dk (A. Hall), moien.moghimi@sund.ku.dk (S.M. Moghimi).

http://dx.doi.org/10.1016/j.bbabio.2014.12.002
0005-2728/

1. Introduction

Polyethylenimines (PEIs) are among the most prominent polycationic non-viral gene delivery systems described to date in compacting nucleic acids and transfecting a wide range of mammalian cell types [1–8]. PEIs exist in either branched or linear architecture and are available in different molecular weights [3,7,9]. It is generally accepted that the higher molecular weight PEIs (25 kDa being the gold standard) are not only more efficient transfection agents than the lower molecular weight counterparts, but also more cytotoxic [3, 10–12]. Furthermore, various in vitro and in vivo studies have suggested that the transfection efficacy of linear PEIs is superior to polycations with branched morphology and of equal molecular weight [13–15], however, the impact of PEI architecture on cytotoxic responses as well as the underlying molecular basis still remain unknown. Previous studies have indicated that PEI-mediated cell death is dynamic and manifests through apoptosis, necrosis or autophagy [11,12,16–19], conceivably as a result of biomembrane destabilization, mitochondrial dysfunction and integrated bioenergetic crisis [2,12,20].

The integrated process of mitochondrial respiration is referred to as oxidative phosphorylation (OXPHOS) [21–23]. Briefly, enzyme-catalyzed substrate oxidation in the tricarboxylic acid cycle (TCA) generates nicotinamide adenine dinucleotide (NADH) and flavin adenine dinucleotide ($FADH_2$), providing a source of electrons for the electron transport system (ETS) through Complex I (CI) and Complex II (CII), respectively. Subsequently, electrons flow from CI and CII via the Q-pool to Complex III (CIII), followed by electron transfer to Complex IV (CIV), also known as cytochrome *c* oxidase, where oxygen acts as the final electron acceptor [22,24]. Electron flow through the ETS is coupled with proton pumping by the inner membrane complexes CI, CIII and CIV, generating an electrochemical proton motive force (Δp), utilized by the mitochondrial F_0/F_1-ATP synthase to produce ATP [21–25]. Insufficient cellular ATP production results in ATP depletion and cellular stress, and fluctuations in ATP levels may induce cell death through various pathways [26–28]. Previously, both linear and branched PEIs were shown to induce mitochondrial depolarization and cytochrome *c* (cyt *c*) release in various human cell lines [11,12,19]. Moreover, we recently demonstrated that cellular exposure to the 25 kDa branched PEI (25 k-PEI-B) initiates gradual time- and concentration-dependent reduction of the Δp and OXPHOS capacity through mild mitochondrial uncoupling and rapid impairment of ETS activity via a potent CIV inhibition [20]. Subsequent to these changes, cells were shown to suffer from bioenergetic crisis, resulting in cell death [20]. Cellular bioenergetic processes are widely interconnected and most cells can fully or partially compensate for decreasing ATP production via OXPHOS by accelerating glycolytic ATP production [29]. Therefore, simultaneous investigations of OXPHOS and glycolysis are more informative in an overall attempt to understand the mechanistic impact of external insults (such as PEI exposure) on cellular bioenergetics.

In addition to producing ATP, OXPHOS generates reactive oxygen species (ROS) as a by-product [30,31]. The latter is formed mainly through electron leakage at CI and CIII, resulting in oxidative stress that may induce a cytotoxic response [31–33]. To counteract oxidative stress, the cell utilizes endogenous antioxidant glutathione (GSH) for restoration of redox homeostasis [34,35]. In the process, GSH is oxidized to GSH disulfide (GSSG), requiring the activity of glutathione reductase for NADPH dependent conversion of GSSG back to GSH, in order to re-establish the cellular redox capacity [34]. Either a decline in intracellular NADPH levels or an overwhelming increase of ROS can exceed the cell's ability to reduce GSSG to GSH, resulting in depletion of intracellular GSH [35]. Enzymes in the pentose phosphate pathway (PPP) and in mitochondrial–cytosolic NADP-linked pathways, involving isocitrate dehydrogenases (IDHs) and malic enzyme (ME), are known to be vital for maintaining intracellular NADPH pools, thus demonstrating the importance of functional mitochondria and adequate glycolytic flux through the PPP for redox homeostasis [36–38].

PEIs can perturb biomembranes and modulate transfection efficacy and cell death in a size- and architecture-dependent manner [2,12–15, 20]. Therefore, it would be imperative to analyze the impact of PEI morphology (branched versus linear) and concentration on destabilization of plasma membrane and mitochondrial membranes with consequences on dynamic dimensions of bioenergetic and redox homeostatic processes that modulate cellular responses to injury. Accordingly, the capacity of OXPHOS, mitochondrial proton leak and the activity of the ETS were investigated in intact cells, permeabilized cells, isolated mitochondria and 'broken mitochondria'. The GSH/GSSG ratio, NADPH and ROS levels were used as indicators of intracellular redox status. A better mechanistic understanding of polycation-mediated biomembrane and metabolic perturbation events could open the path for design of safer polymers through assimilated combinatorial and medium/high-throughput chemical/metabolomic approaches.

2. Materials and methods

2.1. Materials

The 25k-PEI-B (dissolved in milli-Q H_2O), Citrate Synthase Assay Kit, NADP/NADPH Quantification Kit and Glutathione Assay Kit were purchased from Sigma-Aldrich (Denmark). The 10k-PEI-B and 25k-PEI-L were purchased from Polysciences (Germany) and dissolved in milli-Q water. The XF Cell Mito Stress Kit and XF Plasma Membrane Permeabilizer (PMP) were purchased from Seahorse Bioscience (Denmark). The ATPlite luminescence assay system was purchased from Perkin Elmer (Skovlunde, Denmark). All other compounds were purchased from Sigma-Aldrich (Denmark).

2.2. Cell culture

H1299 cells (ATCC number: CRL-5803; Sigma-Aldrich) were cultured in Roswell Park Memorial Institute (RPMI) 1640 medium at 37 °C with 0.1 mg/mL penicillin/streptomycin, 2 mM L-Glutamine and 10% v/v FBS in 21% O_2 and 5% CO_2. C2C12 cells (ATCC number: CRL-

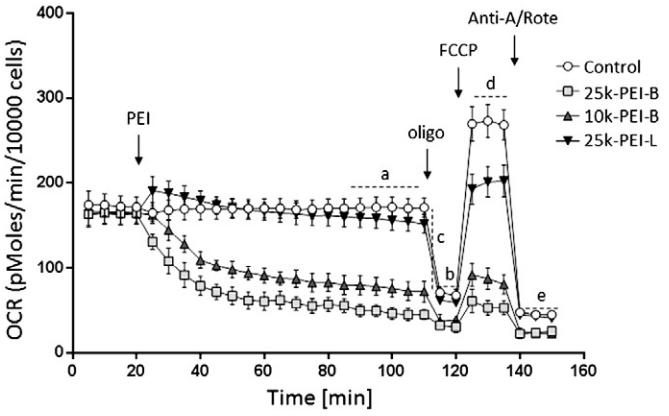

Fig. 1. Representative traces of real-time oxygen consumption rate (OCR) in H1299 cells challenged with 25k-PEI-B (light grey), 10k-PEI-B (dark grey) or 25k-PEI-L (black) at concentration of 4 μg/mL, or without PEI (white). Following PEI exposure (90 min), respiratory states were investigated through sequential additions of different compounds. Oligomycin (oligo) was applied to inhibit mitochondrial F_0/F_1-ATP synthase in order to define non-phosphorylating respiration, representing mitochondrial proton leak across the mitochondrial inner membrane. Next, carbonylcyanide-p-trifluoromethoxyphenylhydrazone (FCCP) was added to obtain the maximum respiratory rate (MRR), indicating the highest capacity of the electron transport system. Finally a combination of rotenone (Rote) and antimycin-A (Anti-A) was used to inhibit the activity of CI and CIII for a measurement of non-mitochondrial respiration. Respiratory states are marked in the figure: basal respiration (a), proton leak (b), oligomycin-sensitive respiration (c = a–b), MRR (d) and non-mitochondrial respiration (e).

1772; Sigma-Aldrich) were cultured in Dulbecco's Modified Eagle's Medium (DMEM) at 37 °C with 0.1 mg/mL penicillin/streptomycin, 2 mM L-Glutamine and 10% v/v FBS in 21% O_2 and 5% CO_2. Cellular quantification assay, ATP, NADPH and ROS measurements, GSH and GSSG quantification experiments, transfection analysis and immunoblot analysis, were performed following exposure of diverse PEIs, at different concentrations and exposure times, in growth medium at 37 °C and at cellular confluence of 60–70%. Regarding experiments using NAC, 5 mM of NAC was applied.

2.3. Cell quantification assay

Cell numbers were examined following PEI exposure by quantification of adherent cells using crystal violet staining procedures [39]. In brief, following PEI exposure cells were washed first with PBS (pH, 7.4) and then fixed with glutaraldehyde for 15 min. Next, cells were stained with crystal violet solution (0.1% crystal violet, 20% CH_3OH) for 1 h and washing in de-ionized water. Thereafter, the dye was extracted by 10% v/v acetic acid for at least 18 h and the absorbance recorded at $\lambda = 595$ nm in a Tecan microplate reader (Infinite M200, Tecan Nordic AB, Sweden).

2.4. Freshly isolated mouse liver mitochondria and freeze–thawed mitochondrial preparation ('broken mitochondria')

Mouse liver mitochondria were isolated from young female NMRI mice (approximately 8–12 weeks old and 35–40 g in body weight) as previously described [20]. 'Broken mitochondria' were obtained by three freezing–thawing cycle disruption of isolated mouse liver mitochondria as reported earlier [20]. The activity of CIV following PEI exposure was monitored in 'broken mitochondria' with high-resolution respirometry (OROBOROS Oxygraph-2k, Innsbruck, Austria) as described in detail elsewhere [20].

2.5. Real-time investigations of OCR and ECAR

Analyses of bioenergetic processes were performed in intact cells, permeabilized cells and freshly isolated mouse liver mitochondria by using XF96 extracellular flux analyzer with XF96 V3 cell culture microplates (Seahorse Bioscience). Cells were seeded in XF96 V3 cell culture microplates at a density of 1×10^4 cells/well in growth medium the day before. Depending on the type of the experiment, the effect of PEI exposure on OCR and ECAR in intact cells were investigated at 37 °C in either Seahorse assay buffer (containing 10 mM glucose, 10 mM pyruvate, at pH 7.4) or basic DMEM medium (containing 10 mM glucose, pH 7.4). Mitochondrial respiratory states, respiratory control ratio (RCR) and coupling efficiency of OXPHOS were investigated according to a previously validated protocol [24,40]. The following compounds and concentrations were added depending on type of the experiment: oligomycin A (1 μM); FCCP (optimized concentrations of 0.9 μM for H1299 cells and 1.0 μM for C2C12, respectively); antimycin-A (2.5 μM); rotenone (2.5 μM); 2-deoxyglucose (50 mM).

2.6. Mitochondrial activity in permeabilized cells

The effect of PEI exposure on mitochondrial activity in permeabilized cells was investigated in mitochondrial respiratory medium (MAS) containing sucrose (70 mM), mannitol (220 mM), KH_2PO_4 (10 mM), $MgCl_2$ (5 mM), HEPES (2 mM), EGTA (1 mM), 0.2% (w/v) BSA free of fatty acids, at pH 7.4 and 37 °C, and in the presence of succinate (10 mM) and rotenone (2.5 μM). Briefly, prior to investigation, cells were exposed to different concentrations of structurally diverse PEIs for 15 min. Subsequent to PEI exposure a saturating concentration of ADP (4 mM) was added together with XF Plasma Membrane Permeabilizer (PMP, 1 nM) for controlled plasma membrane permeabilization and estimation of mitochondrial ATP synthesis. Thereafter, ATP synthase was inhibited by addition of oligomycin (1 μM) for detection of mitochondrial proton leak (LEAK respiration). Next, antimycin-A (2.5 μM) was added for measurement of non-mitochondrial respiration. The OXPHOS capacity for ATP production (oligomycin-sensitive respiration) was calculated as the difference between maximum ADP-stimulated respiration and LEAK respiration.

2.7. Activity of freshly isolated mouse liver mitochondria

The effect of PEI exposure on mitochondrial activity in freshly isolated mouse liver mitochondria was investigated in mitochondrial respiratory medium (MAS) containing sucrose (70 mM), mannitol (220 mM), KH_2PO_4 (10 mM), $MgCl_2$ (5 mM), HEPES (2 mM), EGTA (1 mM) and 0.2% (w/v) BSA free of fatty acids, at pH 7.4 and 37 °C. Isolated mitochondria was loaded in XF96 V3 cell culture microplates at 2.5 μg/well, and the plate was centrifuged at 2000 ×*g* for 10 min at 4 °C, to adhere mitochondria to the plate. Briefly, prior to investigation, isolated mitochondria were challenged with different concentrations of structurally diverse PEIs for 15 min. Leak respiration (state 2) was first investigated in the presence of respiratory substrates (5 mM glutamate and 5 mM malate, or 10 mM succinate and 2.5 μM rotenone) before the addition of a saturating concentration of ADP (4 mM) which results in maximum ADP-stimulated respiration (state 3) and ATP synthesis by the mitochondrial F_0/F_1-ATP synthase. Thereafter, oligomycin was added to inhibit ATP synthase and to achieve non-phosphorylating leak respiration (state 4o). Finally, non-mitochondrial respiration was obtained through combined addition of rotenone (2.5 μM) and antimycin-A (2.5 μM). OXPHOS capacity (oligomycin-sensitive respiration) was calculated as the difference between state 3 respiration and state 4o respiration.

2.8. Western blotting

Lysates from human H1299 NSCLC and mouse myoblast C2C12 cell lines were produced after treatment with PEIs for 30 min and 2 h, respectively. Medium was aspirated and cells washed twice with ice-cold Dulbecco's Phosphate Buffered Saline [–] $CaCl_2$ [–] $MgCl_2$ (Gibco^R by life technologies) and then scraped off the plastic in the presence of RIPA buffer (150 mM NaCl, 1% IGEPAL CA 6305, 0.5% (w/v) sodium deoxycholate, 0.1% (w/v) SDS and 50 mM Tris pH 8) supplemented with a protease inhibitor cocktail (Complete™) and phosphatase inhibitors (PhosSTOP™). Extracts were snap-frozen in liquid nitrogen and stored at −80 °C until use. The protein content was measured using Protein Assay Dye Reagent (Bio-Rad). Next, 50 μg protein from H1299 cell line and 100 μg from C2C12 cell line was separated on NuPage™ 4–12% Bis–Tris polyacrylamide gels (Invitrogen) using NuPage™ MOPS SDS Running Buffer and NuPage™ Antioxidant (Invitrogen™). Antibodies used were as follows: rabbit anti-phosphorylated AMPKα (P-Thr172) (Cell Signaling #2535), rabbit AMPKα (Cell Signaling #2603) and rabbit β-Actin (13E5) (Cell Signaling # 4970).

2.9. ATP measurements

The concentration of ATP was determined using a modified method based on the ATPlite™ luminescence assay system. Briefly, cells were incubated for 2 or 4 h with different PEIs at different concentrations. Samples were collected by lysing the cells with 750 μL lysis solution (2:1 medium:cell lysis buffer) (ATPlite™, Perkin Elmer). Extracellular ATP levels were determined through measurements of ATP concentrations in growth medium following cellular exposure to different concentrations of PEIs at selected time points. ATP levels were measured based on triplicate aliquots taken from the sample in 3:1 ratio with substrate solution (ATPlite™, Perkin Elmer). Luminescence was recorded in a Tecan microplate reader (Infinite M200, Tecan Nordic AB, Sweden) and ATP levels were normalized for protein content determined using Bradford assay.

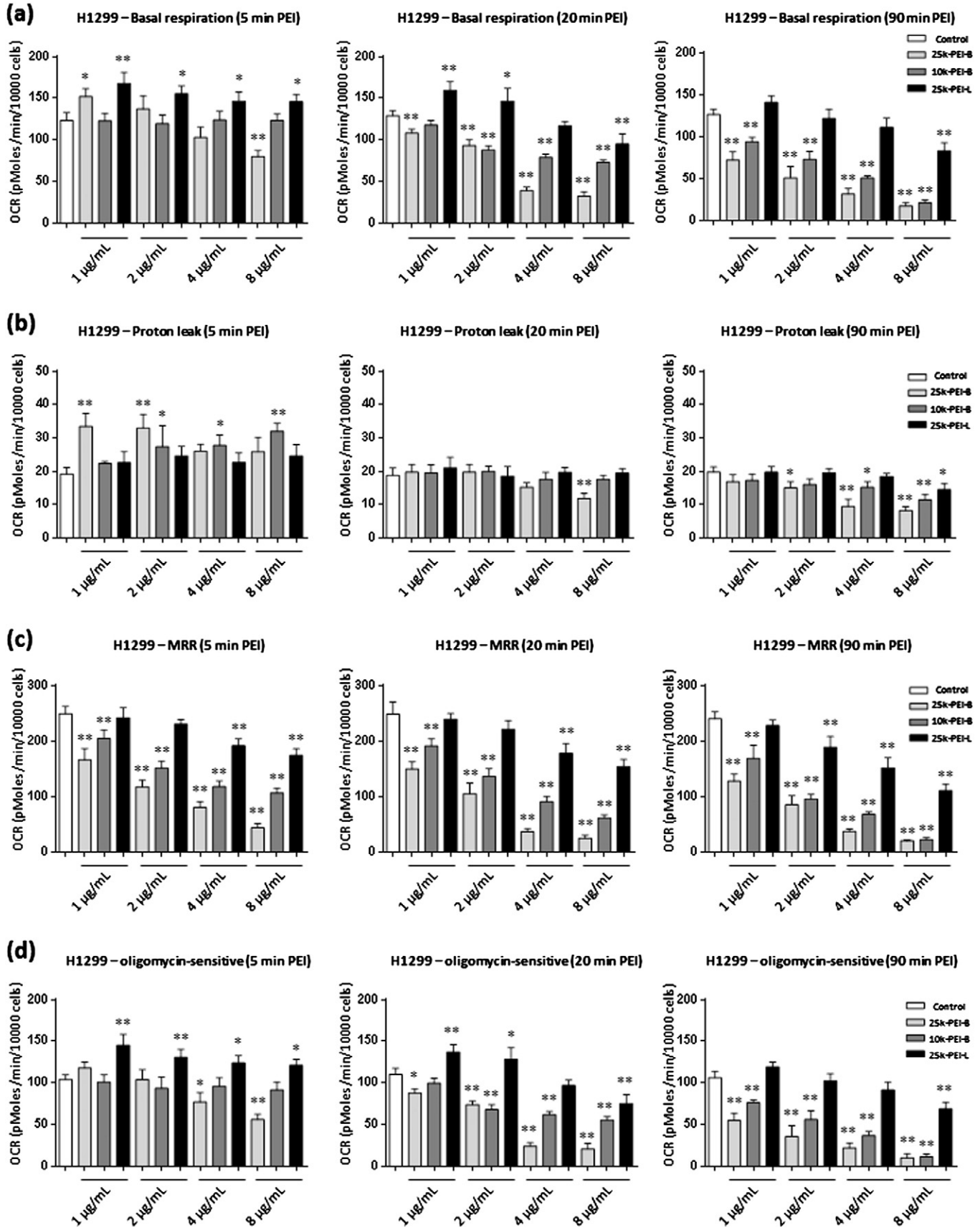

Fig. 2. The effects of PEI concentration and exposure time on respiratory states in intact H1299 cells. In all panels the white open columns represent untreated control incubation and light grey, dark grey and black columns represent 25k-PEI-B, 10k-PEI-B and 25k-PEI-L, respectively. (a) Basal respiration, (b) proton leak, (c) maximum respiratory rate (MRR), and (d) oligomycin-sensitive respiration. OCR (pmol/min/10,000 cells) is corrected for non-mitochondrial respiration. Data are presented as the mean (n = 6) ± SD and statistical analysis was performed using one-way ANOVA and Tukey's multiple comparisons test (*$p < 0.05$; **$p < 0.01$).

2.10. Lactate dehydrogenase (LDH) release assay

Lactate dehydrogenase (LDH) release was investigated at different time points following exposure to different concentrations of PEIs. LDH measurements were performed with CytoTox96 Non-Radioactive Cytotoxicity Assay kit (Promega). The maximum amount of LDH in the cells was measured (following addition of lysis solution) and presented as 100% LDH release. The PEI-induced LDH release as well as to spontaneous cellular LDH release (untreated cells) were compared with the total LDH release and presented as %LDH relative to the total amount of intracellular LDH.

2.11. Enzyme activity assays

Citrate Synthase Assay Kit (Sigma-Aldrich) was used to investigate the effect of PEI exposure on mitochondrial inner membrane integrity in freshly isolated mouse liver mitochondria. Briefly, isolated mitochondria (250 μg protein/mL) were incubated with different concentrations of diverse PEIs for 20 min at room temperature in mitochondrial respiratory medium (MAS) containing sucrose (70 mM), mannitol (220 mM), KH_2PO_4 (10 mM), $MgCl_2$ (5 mM), HEPES (2 mM), EGTA (1 mM) and 0.2% (w/v) BSA free of fatty acids, at pH 7.4. Thereafter, samples were centrifuged at 9000 ×*g* for 5 min at 4 °C in order to separate mitochondria from the supernatant. CS activity was measured in the supernatant at λ = 412 nm in a Tecan microplate reader (Infinite M200, Tecan Nordic AB, Sweden) according to manufacturer's instructions.

NADPH levels were quantified with NADP/NADPH Quantification Kit (Sigma-Aldrich). Briefly, cells were washed twice with cold PBS, scraped and extracted in NADP/NADPH extraction buffer and by two freeze–thawing cycles. Afterward, samples were centrifuged at 13,000 ×*g* for 10 min. The NADP was decomposed by heating samples at 60 °C for 30 min. The NADPH levels in the supernatants were quantified with a colorimetric assay at λ = 450 nm in a Tecan microplate reader (Infinite M200, Tecan Nordic AB, Sweden) and the NADPH concentration (nmol/μg protein) was calculated according to the manufacturer's instruction. Total protein contents of the samples were determined using Bradford assay.

GSH and GSSG levels were investigated using Glutathione Assay Kit (Sigma-Aldrich). Briefly, cells were washed twice with cold PBS, scraped and deproteinized in 5% 5-sulfosalicylic acid solution followed by two freeze–thawing cycles. Then samples were centrifuged at 10,000 ×*g* for 10 min. The supernatants were removed for analysis according to the manufacturer's instruction. Determination of GSSG levels was performed after derivatization of GSH by addition of 2 μL of 2-

Table 1
Respiratory control ratio and coupling efficiency of OXPHOS in H1299 and C2C12 cells following PEI exposure.

Respiratory control ratio	H1299 cells			C2C12 cells		
Time [min]	5	20	90	5	20	90
Control	13.2 ± 1.0	13.3 ± 0.5	12.2 ± 1.1	14.8 ± 1.8	15.1 ± 1.5	15.4 ± 1.2
25 k-PEI-B						
1 μg/mL	7.7 ± 1.4 *	7.6 ± 0.8 *	5.2 ± 0.7 **	9.7 ± 1.8 *	9.5 ± 1.3 *	8.5 ± 1.4 *
2 μg/mL	5.7 ± 0.9 **	5.3 ± 1.0 **	3.8 ± 0.6 **	8.2 ± 0.9 *	6.1 ± 0.8 **	6.3 ± 1.1 **
4 μg/mL	4.2 ± 1.4 **	2.9 ± 0.5 **	2.5 ± 0.3 **	5.6 ± 0.5 **	5.3 ± 0.8 **	4.8 ± 0.4 **
8 μg/mL	2.5 ± 0.4 **	2.4 ± 0.7 **	1.8 ± 0.4 **	5.0 ± 1.3 **	3.6 ± 0.5 **	3.3 ± 0.5 **
10k-PEI-B						
1 μg/mL	10.1 ± 1.6	9.9 ± 2.0	9.2 ± 0.7	14.4 ± 0.9	15.4 ± 2.1	15.6 ± 1.5
2 μg/mL	7.1 ± 0.5 *	5.7 ± 0.8 **	5.7 ± 1.2 **	11.8 ± 1.9	10.6 ± 1.2 *	9.5 ± 1.0 *
4 μg/mL	5.1 ± 0.7 **	4.8 ± 1.0 **	4.3 ± 0.2 **	8.3 ± 1.5 *	7.1 ± 1.1 **	6.1 ± 0.9 **
8 μg/mL	3.5 ± 0.6 **	3.3 ± 0.5 **	2.2 ± 0.5 **	6.7 ± 1.1 **	5.8 ± 1.5 **	4.4 ± 0.5 **
25k-PEI-L						
1 μg/mL	11.2 ± 1.1	11.6 ± 1.6	11.5 ± 0.6	15.5 ± 1.3	15.0 ± 0.8	14.7 ± 0.9
2 μg/mL	12.2 ± 2.8	9.7 ± 1.2	9.5 ± 1.4	14.1 ± 2.1	14.5 ± 1.6	13.5 ± 1.4
4 μg/mL	9.1 ± 1.2	8.4 ± 0.8 *	8.2 ± 0.6 *	13.2 ± 1.5	11.3 ± 0.8	12.7 ± 1.2
8 μg/mL	7.8 ± 1.2 *	7.8 ± 0.6 *	7.2 ± 0.8 *	13.1 ± 1.0	9.6 ± 0.7 *	5.0 ± 1.1 **
Coupling efficiency	**H1299 cells**			**C2C12 cells**		
Time [min]	**5**	**20**	**90**	**5**	**20**	**90**
Control	0.83 ± 0.01	0.81 ± 0.01	0.82 ± 0.01	0.90 ± 0.03	0.88 ± 0.03	0.91 ± 0.04
25k-PEI-B						
1 μg/mL	0.76 ± 0.01	0.73 ± 0.03	0.70 ± 0.02 *	0.88 ± 0.02	0.87 ± 0.04	0.86 ± 0.03
2 μg/mL	0.73 ± 0.02	0.70 ± 0.02 *	0.61 ± 0.04 **	0.85 ± 0.04	0.85 ± 0.03	0.84 ± 0.02
4 μg/mL	0.70 ± 0.02 *	0.62 ± 0.03 **	0.51 ± 0.02 **	0.85 ± 0.03	0.83 ± 0.04	0.62 ± 0.05 **
8 μg/mL	0.66 ± 0.02 *	0.53 ± 0.02 **	0.42 ± 0.04 **	0.78 ± 0.03 *	0.70 ± 0.03 **	0.46 ± 0.06 **
10k-PEI-B						
1 μg/mL	0.78 ± 0.02	0.77 ± 0.04	0.74 ± 0.01	0.89 ± 0.03	0.91 ± 0.03	0.90 ± 0.03
2 μg/mL	0.74 ± 0.03	0.73 ± 0.02	0.70 ± 0.02 *	0.87 ± 0.03	0.89 ± 0.02	0.89 ± 0.04
4 μg/mL	0.73 ± 0.01	0.67 ± 0.03 *	0.63 ± 0.02 **	0.84 ± 0.01	0.76 ± 0.02 *	0.61 ± 0.03 **
8 μg/mL	0.70 ± 0.01 *	0.61 ± 0.02 **	0.49 ± 0.04 **	0.86 ± 0.04	0.74 ± 0.04 *	0.58 ± 0.05 **
25k-PEI-L						
1 μg/mL	0.82 ± 0.01	0.83 ± 0.03	0.81 ± 0.02	0.91 ± 0.04	0.88 ± 0.04	0.89 ± 0.02
2 μg/mL	0.83 ± 0.03	0.84 ± 0.02	0.82 ± 0.01	0.89 ± 0.02	0.92 ± 0.05	0.91 ± 0.05
4 μg/mL	0.82 ± 0.02	0.78 ± 0.03	0.78 ± 0.01	0.92 ± 0.01	0.91 ± 0.03	0.92 ± 0.03
8 μg/mL	0.81 ± 0.03	0.73 ± 0.01	0.71 ± 0.02 *	0.88 ± 0.02	0.87 ± 0.04	0.75 ± 0.04 *

Respiratory control ratio (RCR) and coupling efficiency of OXPHOS are calculated from the data in Fig. 2 and Supplementary Figure S4 and is presented as the means ± SD (n = 6). The RCR is the ratio of maximum respiratory rate (MRR) and mitochondrial proton leak (RCR = MRR/proton leak). The RCR gives an estimate of the mitochondrial capacity for oxidation of respiratory substrates and ATP synthesis. The coupling efficiency of OXPHOS is calculated as the ratio between basal respiration and oligomycin-sensitive respiration and denotes the fraction of protons being used by the ATP synthase for generation of ATP relative to the fraction of protons leaking over the mitochondrial inner membrane (oligomycin-sensitive respiration/basal respiration). Statistical analyses were performed with one-way ANOVA, using Tukey's multiple comparisons correction to calculate significance (* $p < 0.05$; ** $p < 0.01$).

vinylpyridine (Sigma-Aldrich) per 100 μL sample. Total GSH and GSSG levels were determined according to the manufacturer's instruction at λ = 412 nm in a Tecan microplate reader (Infinite M200, Tecan Nordic AB, Sweden). GSH and GSSG levels were normalized for protein content determined using Bradford assay.

2.12. ROS measurements

General levels of ROS were measured using the fluorescent probe 5,6-carboxy-2′,7′-dichlorodihydrofluorescein diacetate (carboxy-H_2DCFDA) (Invitrogen). Briefly, 100,000 cells were seeded in normal medium in small tissue culture flasks two days before measurement. On the analysis day, the flasks were first pretreated for one hour with 5 mM N-acetylcysteine when appropriate, and then either treated with 8 μg/mL PEI, antimycin A plus rotenone (5 μM each) or 50 μM tert-butyl hydroperoxide (TBHP) for 2 h. Medium was then changed to DME/F12 medium containing 1% v/v FBS and 10 μM carboxy-H_2DCFDA and cells incubated for a further 30 min. Finally, cells were trypsinized and washed in PBS containing 1% v/v FBS and the amount of intracellular ROS measured in a FACSCalibur™ flow cytometer using the Argon Ion laser and FL1 green emission filter.

2.13. Polyplex formation

25k-PEI-B and 10k-PEI-B were complexed with plasmid DNA and characterized as previously described [1]. Briefly, PEI and DNA (pcDNA3-EGFP) were diluted in 150 mM NaCl. PEI was then added to DNA (1.8 μg/mL DNA/well) at N/P = 7 during vortexing and left at room temperature for 10 min prior to addition to cells.

2.14. Transfection efficiency

H1299 and C2C12 cells were seeded in 12 well plates (20×10^3 cells/well) and grown for 2 days. On the day of treatment the cell medium was replaced with fresh medium. Cells were then treated with NAC (5 mM) and PEI:DNA polyplexes and incubated (37 °C, 5% CO_2) for 48 h. Following incubation the cell medium was collected and cells were washed in PBS and detached by trypzination (0,5 g/L Porcine trypsin, 0,2 g/L EDTA, 0,09% sodium chloride). The collected culture medium and the detached cells were centrifuged at 800 × g for 10 min and the resulting pellet was resuspended in 250 μL PBS. The percentage of GFP expressing cells in the FL-1 channel and the gated healthy population were analyzed by flow cytometry on BD FACS array.

2.15. Statistical analysis

Results are expressed as the means and SD from at least three independent experiments except stated otherwise. Statistical analysis of multiple groups was performed with one-way ANOVA and Tukey's multiple comparison method. Statistical analysis between two groups was performed with paired student *t*-test. Values of $p < 0.05$ were considered significant.

3. Results

3.1. Morphologically diverse PEIs show differential impact on mitochondrial respiration

Here we have focused on two validated cellular models that have been used in studies of bioenergetics and mitochondrial poisons (the human

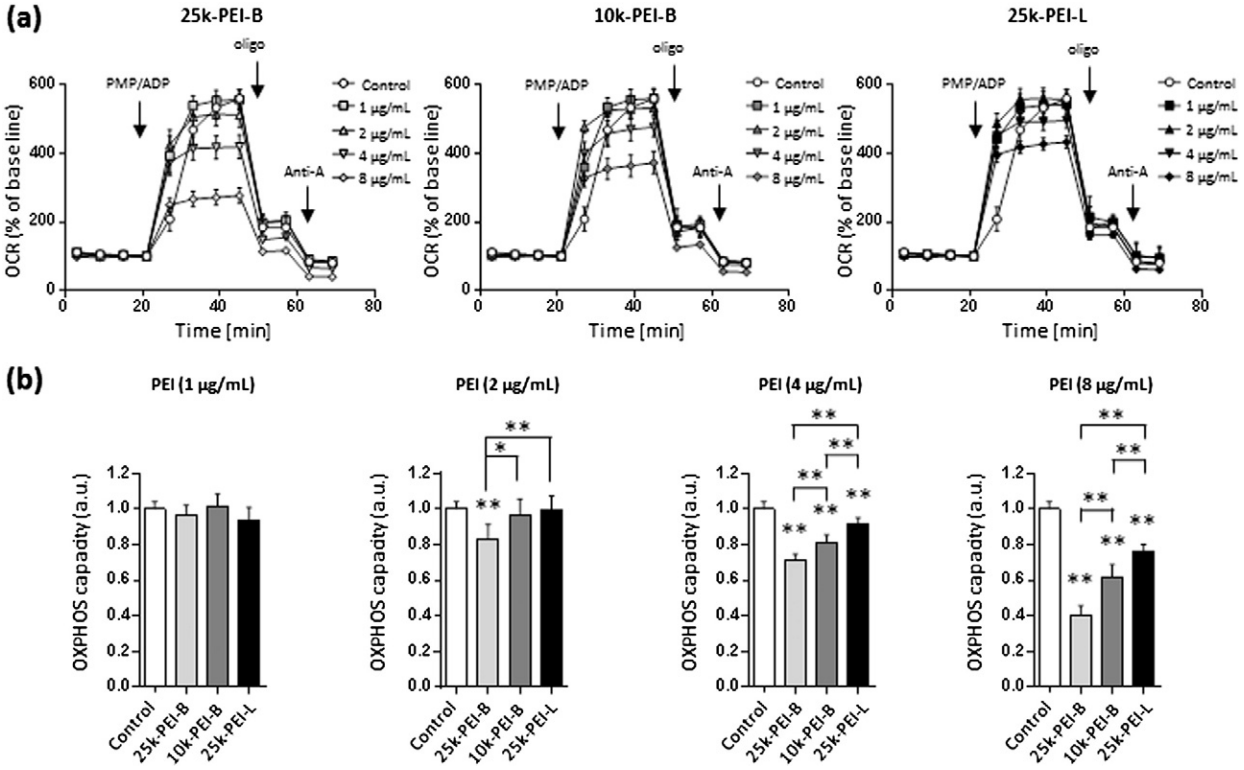

Fig. 3. OXPHOS capacity in permeabilized C2C12 cells following exposure to different PEIs. (a) Representative traces of OCR (% of baseline) in MAS buffer in the presence of succinate (10 mM), rotenone (2.5 μM) and different concentrations of PEIs. Following PEI exposure, addition of 1 nM PMP (plasma membrane permeabilizer) and ADP (4 mM) was made to initiate OXPHOS. Next, oligomycin (oligo; 1 μM) was applied to inhibit F_0/F_1-ATP synthase for evaluation of leak respiration. Thereafter, antimycin-A (Anti-A; 2.5 μM) was added to inhibit electron flow through CIII. (b) Relative OXPHOS capacity (oligomycin-sensitive respiration) in permeabilized C2C12 cells following PEI exposure. Columns: 25 k-PEI-B (light grey), 10 k-PEI-B (dark grey) and 25 k-PEI-L (black). Data are presented as the mean (n = 6) ± SD and statistical analysis was performed using one-way ANOVA and Tukey's multiple comparisons test (*$p < 0.05$; **$p < 0.01$).

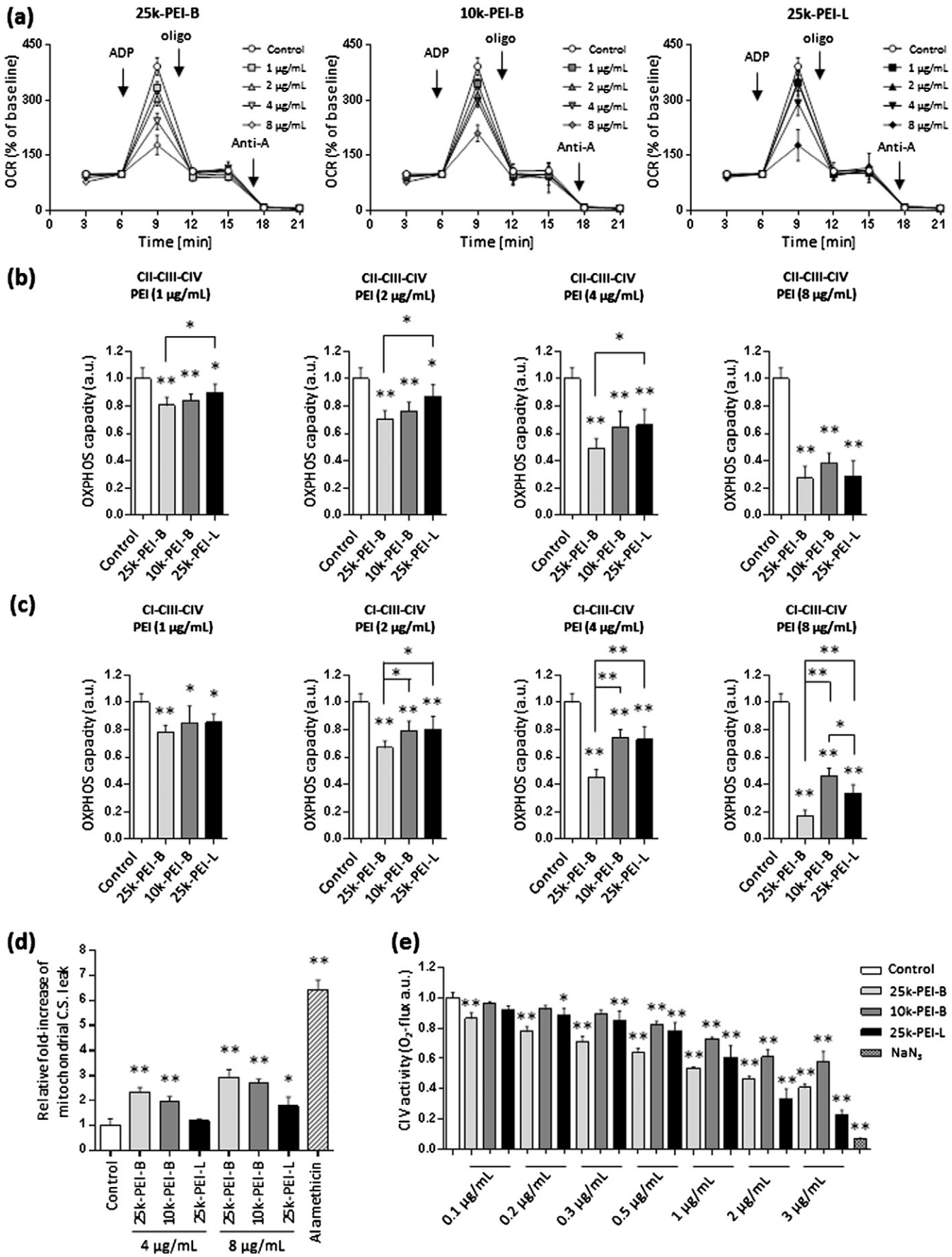
(a)
25k-PEI-B
10k-PEI-B
25k-PEI-L
ADP
oligo
Anti-A
Control
1 μg/mL
2 μg/mL
4 μg/mL
8 μg/mL
OCR (% of baseline)
Time [min]
(b)
CII-CIII-CIV
PEI (1 μg/mL)
PEI (2 μg/mL)
PEI (4 μg/mL)
PEI (8 μg/mL)
OXPHOS capacity (a.u.)
Control
25k-PEI-B
10k-PEI-B
25k-PEI-L
(c)
CI-CIII-CIV
PEI (1 μg/mL)
PEI (2 μg/mL)
PEI (4 μg/mL)
PEI (8 μg/mL)
(d)
Relative fold-increase of mitochondrial C.S. leak
4 μg/mL
8 μg/mL
Alamethicin
(e)
CIV activity (O_2 flux a.u.)
NaN_3
0.1 μg/mL
0.2 μg/mL
0.3 μg/mL
0.5 μg/mL
1 μg/mL
2 μg/mL
3 μg/mL

non-small cell lung carcinoma cell line H1299 and the skeletal myoblasts C2C12) [20,41]. We started by investigating the effects of PEI architecture and concentration on cell numbers. Compared with linear 25 kDa PEI (25k-PEI-L), cellular exposure to branched PEIs of either 10 kDa (10k-PEI-B) or 25 kDa (25k-PEI-B) resulted in higher overall reduction in the number of H1299 and C2C12 cells (Supplementary Figure S1).

Next, we studied the time- and concentration-dependent effect of PEI architecture on mitochondrial respiratory states in intact cells through real-time measurements of oxygen consumption rate (OCR) by utilizing the cell respiratory control protocol [24,40]. Fig. 1 illustrates the experimental protocol and defines individual respiratory states (representative traces of OCR measurements are presented in Supplementary Figures S2 & S3). The results in Fig. 2a and Supplementary Figure S4a depict changes in basal respiration following PEI exposure in the two cell lines. In H1299 cells, 25k-PEI-B, at a low concentration (1 μg/mL), significantly increased OCR within 5 min of exposure, whereas at higher concentrations (8 μg/mL), there was an immediate and significant decrease in OCR. With longer exposure times (20 and 90 min), OCR was gradually reduced with all tested PEI concentrations, but the effect was more pronounced with increasing the polycation concentration (Fig. 2a). On the other hand, exposure of C2C12 cells to 25k-PEI-B at concentrations of 1–4 μg/mL resulted in an early (5 min) increase in OCR, however, at longer exposure times (20 and 90 min), polycation concentrations of 2–8 μg/mL was sufficient to significantly decrease OCR (Supplementary Figure S4a). The 10k-PEI-B affected basal respiration in a similar manner to 25k-PEI-B in both cell lines, however, higher concentrations of 10 k-PEI-B were needed to obtain the same degree of OCR reduction as seen with 25k-PEI-B, and in H1299 cells, 10k-PEI-B did not increase OCR at early time points (5 min) (Fig. 2a & Supplementary Figure S4a). In contrast to branched PEIs, 25k-PEI-L significantly increased OCR at early time points (within 5 min) in both cell lines, but OCR did not decline as rapidly as seen with branched polycations. Lower OCR was only observed with 25k-PEI-L at 8 μg/mL for 20 and 90 min exposure time in H1299 cells, and at 90 min with 8 μg/mL in C2C12 cells (Fig. 2a & Supplementary Figure S4a).

Besides changes in basal respiration, exposure to branched PEIs significantly increased mitochondrial proton leak in both cell lines at early time points (5 min), but this was followed by decreasing proton leak in a concentration-dependent manner (Fig. 2b & Supplementary Figure S4b). In contrast to the branched species, 25k-PEI-L initiated less alteration of proton leak (Fig. 2b & Supplementary Figure S4b). Subsequently, we investigated the maximum respiratory rate (MRR) to assess the maximum activity of the ETS following PEI exposure. In both cell lines, all three types of PEI reduced MRR in a concentration- and time-dependent manner, although to different degrees (Fig. 2c & Supplementary Figure S4c). In contrast to the linear polycation, the branched forms of PEI (25k-PEI-B and 10k-PEI-B) were found to be effective inhibitors of MRR, with the 25k-PEI-B being most potent.

Next, we calculated the effect of PEI exposure on oligomycin-sensitive respiration (mitochondrial ATP synthesis). In C2C12 cells, oligomycin-sensitive respiration was significantly increased after 5 min of exposure to branched PEIs (Supplementary Figure S4d), but gradually declined in both cell lines (20 and 90 min) in a concentration-dependent manner (Fig. 2d & Supplementary Figure S4d). In contrast, exposure to the linear PEI increased oligomycin-sensitive respiration in both cell lines at 5 min with all tested concentrations, and the increase in respiration remained stable over longer periods of time (Fig. 2d & Supplementary Figure S4d). However, at later time points (between 20–90 min in H1299 cells and 90 min in C2C12 cells) a higher concentration (8 μg/mL) of the linear polycation was required to decrease oligomycin-sensitive respiration.

To obtain comparable estimates of mitochondrial efficiency in cells following PEI exposure, we subsequently calculated the mitochondrial respiratory control ratio (RCR) and the coupling efficiency of OXPHOS (Table 1). This was based on the analysis of the mitochondrial respiratory states (Fig. 2 & Supplementary Figure S4) in accordance with previous studies [39,40]. The RCR indicates the mitochondrial capacity for oxidation of respiratory substrates and ATP synthesis, whereas the coupling efficiency of OXPHOS denotes the fraction of protons being used by the F_0/F_1-ATP synthase for the generation of ATP relative to proton leak across the mitochondrial inner membrane. Indeed, all three forms of PEIs significantly reduced both the RCR and the coupling efficiency of OXPHOS in a time- and concentration-dependent manner (Table 1). The branched polycations were generally more potent than the linear species and the larger branched PEI (25 kDa) was more detrimental to mitochondrial functions than the smaller counterpart (10k-PEI-B).

Next we studied the effect of PEI exposure on mitochondrial function through analysis of OXPHOS capacity in cells following controlled plasma membrane permeabilization [24] (Supplementary Figures S5–S7). All types of PEIs reduced the OXPHOS capacity in a concentration-dependent manner, but in comparison with linear PEI, the branched molecules were more potent inhibitors of OXPHOS capacity (Fig. 3). Investigations of PEI exposure to freshly isolated mouse liver mitochondria further showed that both linear and branched PEIs inhibit OXPHOS capacity (Fig. 4a & b & c & Supplementary Figures S8–S10) and induce proton leak (state 2 and state 4o respiration) (Supplementary Figures S11 & S12), and citrate synthase (CS) leak across the mitochondrial inner membrane (Fig. 4d) in a concentration-dependent manner, with the 25 k-PEI-B being the most potent polycation. Interestingly, experiments with 'broken mitochondria' (freeze-thawed mitochondrial preparation) showed that all PEIs inhibited CIV at very low concentrations (0.1–0.5 μg/mL), although 25 k-PEI-B again was most potent (Fig. 4e). However, with increasing PEI concentrations (1–3 μg/mL), the inhibitory effect of the linear PEI approaches and surpasses that of the branched architecture (Fig. 4e).

Collectively, the above experiments indicate that structurally diverse PEIs, in a concentration-dependent manner, impair the mitochondrial OXPHOS capacity and inhibit CIV activity differentially, with the 25 kDa branched PEI being more potent than its linear counterpart at low concentrations. Furthermore, the data suggest that with increased accessibility to mitochondria (permabilized cells, isolated mitochondria and 'broken mitochondria'), the detrimental effect of the linear PEI approaches that of the branched polycations.

3.2. PEIs affect the overall bioenergetics in an architecture-dependent manner

Mitochondrial dysfunction can give rise to increased glycolytic flux to maintain ATP production in response to reduced OXPHOS capacity [29]. Therefore, simultaneous measurement of both OCR and extracellular

Fig. 4. OXPHOS capacity in freshly isolated mouse liver mitochondria proceeding PEI exposure. (a) Representative traces of OCR (% of baseline) in MAS buffer in the presence of CII substrate (10 mM succinate) together with rotenone (2.5 μM) for CI inhibition, in combination with different concentrations of PEIs. Following PEI exposure, ADP (4 mM) was added to initiate state 3 respiration. Next, oligomycin (oligo; 1 μM) was applied to inhibit F_0/F_1-ATP synthase for evaluation of leak respiration (state 4o). Thereafter, antimycin-A (Anti-A; 2.5 μM) was added to inhibit electron flow through CIII. (b) OXPHOS capacity (state 3–state 4o) following PEI exposure, in the presence of CII substrates and electron flow through the CII–CIII–CIV. (c) OXPHOS capacity (state 3–state 4o) following PEI exposure, in the presence of CI substrates (10 mM glutamate and 10 mM malate) and electron flow through the CI–CIII–CIV. Data are presented as the mean ($n = 6$) ± SD and statistical analysis was performed using one-way ANOVA and Tukey's multiple comparisons test (*$p < 0.05$; **$p < 0.01$). (d) The leak of citrate synthase (C.S.) from mitochondria following exposure to different PEIs (4 or 8 μg/mL). Treatments with the pore-forming peptide alamethicin (20 μg/mL) (hatched column) or without PEI (white column) were used as controls. Data are presented as the fold-difference in relation to non-treated control ($n = 5$) and statistical analysis was performed using one-way ANOVA and Tukey's multiple comparisons test (*$p < 0.05$; **$p < 0.01$). (e) The effect of PEI exposure on CIV activity in 'broken mitochondria' in the presence of TMPD (0.5 mM), ascorbate (2 mM), cyt *c* (10 μM), Rote (2.5 μM), malonic acid (5 mM, Mna), Anti-A (2.5 μM) and different concentrations of diverse PEIs. Sodium azide (100 mM, NaN_3) was used as a control to complete CIV inhibition. The columns in (b), (c), (d) and (e) are as follows: 25 k-PEI-B (light grey), 10 k-PEI-B (dark grey) or 25 k-PEI-L (black).

acidification rates (ECAR) enables a more comprehensive assessment of cellular energetics, and provides more detailed insights into the dynamic interplay between these two energy-yielding pathways. Accordingly, we performed parallel investigations of both ECAR and OCR in intact cells at the same time following PEI exposure (Fig. 5a & b & Supplementary Figures S2 & S3). In accordance with investigations into mitochondrial function in intact cells following PEI exposure (Fig. 2 & Supplementary Figures S2–S4), branched PEIs exerted more potent time- and concentration-dependent impairment of OCR compared with the linear counterpart (Fig. 5a & Supplementary Figures S2 & S3). Following PEI addition, ECAR increased in both cell lines, however, subsequent to the initial increase branched PEIs caused a rapid time- and concentration-dependent collapse of ECAR. On the contrary, no reduction was observed in ECAR when cells were exposed to linear PEI (Fig. 5b & Supplementary Figures S2 & S3). As a result of the differences observed between the branched and linear PEIs on the OCR and ECAR, we further investigated the consequential effects of PEI exposure on intracellular ATP levels (Fig. 5c). The 25 k-PEI-B was found to reduce intracellular ATP levels in a time- and concentration-dependent manner in the range of 2–8 μg/mL. The 10k-PEI-B similarly reduced ATP levels in a time- and concentration-dependent manner, although exposure with higher concentrations was needed (4–8 μg/mL). In contrast, exposure with the 25k-PEI-L only resulted in decreased ATP levels at higher concentrations (8 μg/mL), thus reflecting the milder inhibitory effect of the 25k-PEI-L on both OXPHOS capacity and glycolysis. In addition, early time exposure (10–60 min) to higher quantities (4–8 μg/mL) of PEIs increased the extracellular ATP levels in a concentration-dependent manner, a phenomenon which was more prominent with the branched morphology (Supplementary Figure S13). In agreement with our previous study [20], this indicates that plasma membrane destabilization/perturbation events by PEIs are partially responsible for the decline in intracellular ATP levels and particularly at higher polycation concentrations. Moreover, the extracellular ATP levels peaked at 30 min of PEI exposure and thereafter gradually declined (Supplementary Figure S13), although the intracellular ATP levels were not completely depleted (Fig. 5c). This decline in total extracellular ATP levels is presumably due to some ATP hydrolysis (e.g. through a cascade hydrolysis process by ectonucleotidases that are presumably released through PEI-mediated plasma membrane destabilization) and/or indicative of intracellular ATP utilization for membrane repair events, at least with respect to modest levels of injury in some cell populations.

Further experiments, using the non-metabolizable glucose analogue 2-deoxy-D-glucose (2-DG), demonstrated that a large proportion of the branched PEI-mediated reduction of ECAR was, indeed, attributed to decreased glycolytic flux (Fig. 6a). In addition, the initial increase of ECAR following PEI exposure was also found to be due to increased glycolytic activity, presumably as a consequence of PEI-mediated mitochondrial injury and reduced mitochondrial ATP synthesis. Interestingly, cells exposed to the linear PEI were able to sustain a stable increase in glycolytic flux without subsequent collapse at later time points (Fig. 6a). The observed changes in ECAR were not directly linked to potential acidic/alkaline properties of the polycations, since addition of PEIs to the medium without cells had no effect on the pH of the medium (Supplementary Figure S14). Lactate dehydrogenase (LDH) is an important enzyme for glycolytic activity and extracellular release of LDH release is often used as a parameter indicating plasma membrane damage. We found that all types of tested PEIs facilitated LDH release in a time- and concentration-dependent manner, with the branched morphology being more potent than the linear macromolecule (Supplementary Figure S15). Accordingly, lower amount of intracellular LDH might contribute to the collapse of glycolytic activity upon exposure to higher concentrations (4 and 8 μg/mL) of the branched PEIs.

The AMP kinase (AMPK) is a known metabolic regulator and a sensor of bioenergetic stress, which can be activated by ATP deficiency [42]. In line with the observed branched PEI-mediated perturbations of OCR, ECAR and ATP levels, cellular exposure to branched PEIs caused activation of AMPK in both H1299 and C2C12 cells as evident from increased phosphorylation of Thr172 in the alpha subunit of AMPK (Fig. 6b). Overall, the same qualitative effects were observed in both cell lines, however the effects of 25k-PEI-B on ECAR and ATP levels were milder in C2C12 cells (Figs. 5c & 6a), which carried over into a lesser activation of AMPK in these cells (Fig. 6b). Notably, exposure to linear PEI did not result in increased activation of AMPK, which is in agreement with the less detrimental effect of this species on OCR, ECAR and ATP levels in both cell lines (Figs. 5 & 6a & Supplementary Figures S2 & S3). Collectively, these data demonstrate that structurally diverse PEIs affect cellular energy-yielding pathways differentially and that the combined inhibition of OXPHOS and glycolysis by the branched PEIs results in more severe bioenergetic stress than seen with the linear form.

Finally, a purified form of linear PEI (22 kDa) had almost identical impact on OCR and ECAR as the 25k-PEI-L (Supplementary Figures S16 & S17) as well as being less detrimental compared with the branched species (Supplementary Figures S18 & S19). This strongly suggests that the harmful effect of PEIs on bioenergetic processes is a function of their structure and not the presence of low molecular weight amine and other possible impurities and contaminants [43–45].

3.3. The cytotoxicity of branched PEIs is partly due to oxidative stress

Glycolytic flux through the PPP and the activity of NADP-linked enzymes in mitochondria-cytosolic pathways provide essential source of NADPH for various biosynthetic processes [36–38]. Given our observation that structurally diverse PEIs affect glycolytic flux and mitochondrial functions differentially, we investigated the intracellular NADPH levels following PEI exposure. These experiments showed that exposure to branched PEIs results in reduction of NADPH levels (Fig. 6c), whereas exposure to linear PEI did not significantly reduce NADPH (Fig. 6c). This is consistent with the fact that the linear PEI does not impair glycolytic activity (Figs. 5b & 6a) and is also less detrimental to mitochondrial functions in intact cells (Fig. 2 & Supplementary Figure S4). ROS scavenging by GSH is partially dependent on the reductive power stored within NADPH, and the GSH:GSSG ratio is a valid indicator of cellular redox status [34,35]. When NADPH levels decline, the GSH:GSSG ratio is expected to decrease, whereas the ROS level is expected to increase. Indeed, the intracellular GSH:GSSG ratio was decreased following exposure to branched PEIs, whereas no significant differences in the GSH:GSSG ratio were observed on exposure to linear PEI (Fig. 6d). Moreover, ROS levels increased upon branched PEI exposure, but not with the linear PEI (Fig. 7a & b & Supplementary Figure S20). Oxidative stress is a potential cause of cell death across different cell types and treatments [33]. Therefore, we investigated whether treatment with the GSH precursor *N*-acetyl-cysteine (NAC) could attenuate the cytotoxicity of branched PEIs and, concomitantly, improve transfection performance. The results in Fig. 7c & d (also Supplementary Figure S21) show that NAC improved the fraction of adherent H1299 cells, which is also reflected in lesser ROS production (Fig. 7b). In C2C12 cells, NAC treatment significantly reduced the overall ROS generation by 25 k-PEI-B, but the effect was marginal for the lower molecular weight 10 k-PEI-B (Fig. 7b). For either type of branched PEIs, NAC exposure did not apparently improve the total fraction of adherent C2C12 cells (Fig. 7c & d & Supplementary Figure S21), however crystal violet staining is not representative of cellular viability. Interestingly, NAC treatment increased the number of viable H1299 and C2C12 cells that positively expressed GFP on transfection with corresponding polyplexes containing GFP-encoding plasmid DNA (Fig. 7e), thus implying a role for ROS in branched PEI-mediated cellular injury.

4. Discussion

We have unraveled the causal interconnections between PEI architecture-mediated disturbances of bioenergetic processes and

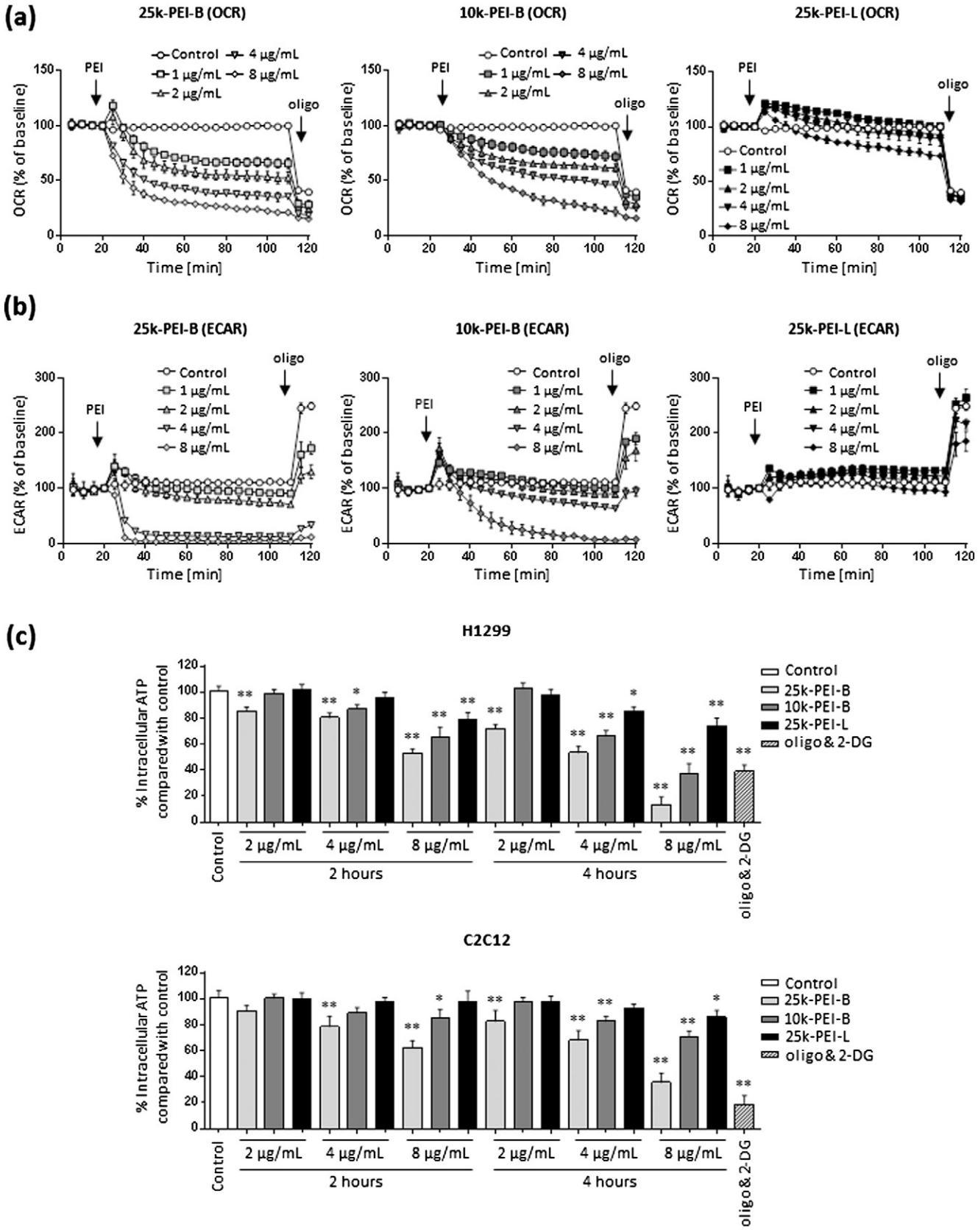

Fig. 5. Representative traces of parallel real-time measurements of (a) OCR and (b) ECAR in H1299 cells following exposure to different concentrations of 25 k-PEI-B (light grey), 10 k-PEI-B (dark grey) or 25 k-PEI-L (black). Oligomycin (oligo; 1 μM) was applied to inhibit F_0/F_1-ATP synthase, causing ATP production to shift primarily to glycolysis. Data are presented as the means (n = 6) ± SD. (c) Intracellular ATP levels in H1299 and C2C12 cells following 2 and 4 h of incubation with different concentrations of 25 k-PEI-B (light grey columns), 10 k-PEI-B (dark grey columns) and 25 k-PEI-L (black columns), respectively. Non-treated cells (white columns) or cells incubated for 2 h with a combination of 2-DG (10 mM) and oligomycin (oligo; 10 μM) (hatched columns) were used as controls. Data are presented as the mean (n = 4) ± SD and statistical analysis was performed using one-way ANOVA and Tukey's multiple comparisons test ($^*p < 0.05$; $^{**}p < 0.01$).

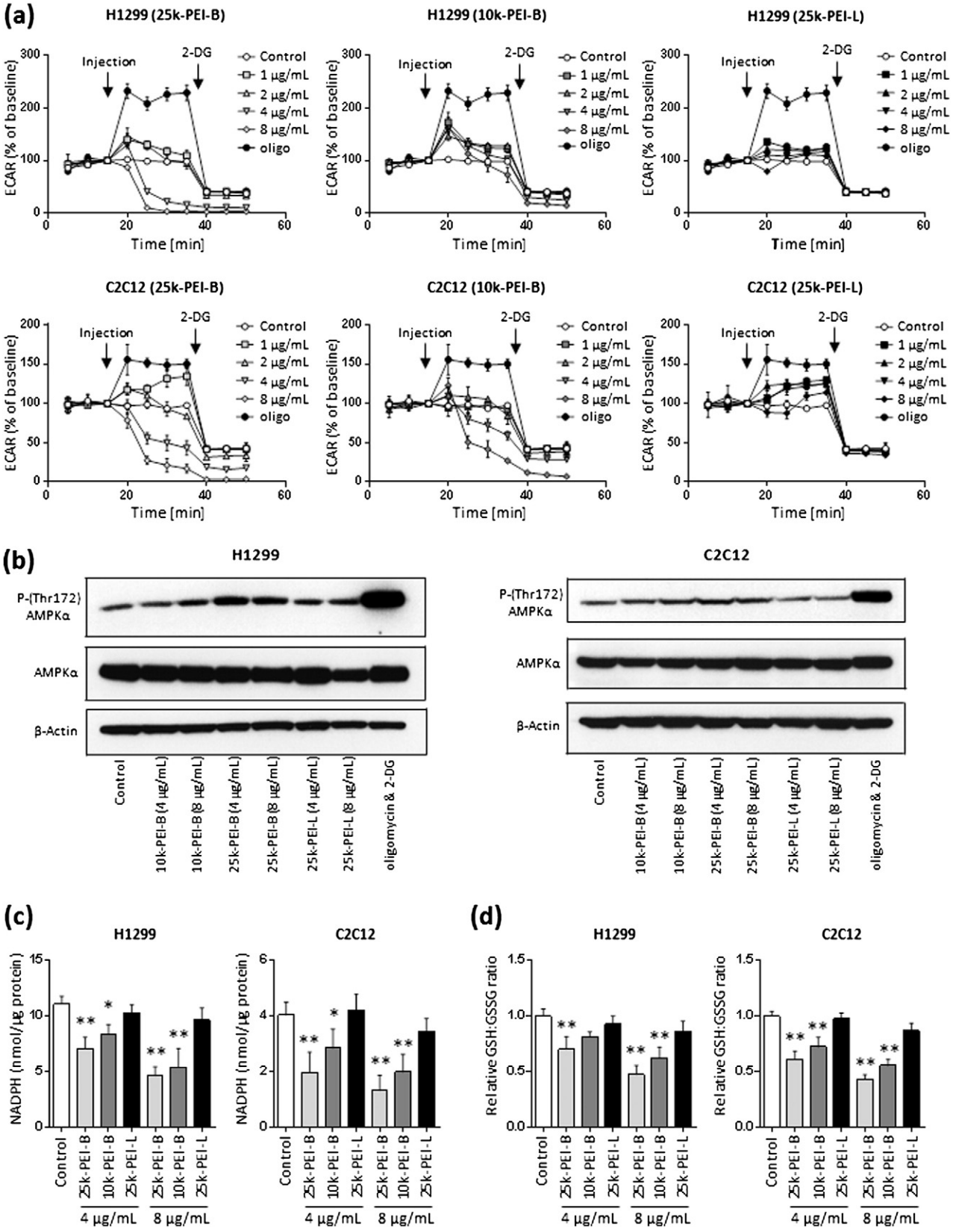

Fig. 6. The effect of PEI architecture and concentration on glycolytic flux, AMPK activation, NADPH levels and GSH:GSSG ratio. Panel (a) shows 2-DG sensitive ECAR in H1299 and C2C12 cells following exposure to different concentrations of 25 k-PEI-B (light grey), 10 k-PEI-B (dark grey) and 25 k-PEI-L (black), respectively. Oligomycin (oligo; 1 μM) was used as a control to inhibit mitochondrial ATP production and to shift energy production primarily to glycolysis. Data are presented as the means ($n = 6$) ± SD. (b) Immunoblot analysis of AMPK activation following exposure to 4 or 8 μg/mL of 25 k-PEI-B, 10 k-PEI-B or 25 k-PEI-L, showing phospho-(Thr172)-AMPKα, total AMPKα and β-actin. Panel (c) shows intracellular NADPH levels in H1299 and C2C12 cells following 2 h exposure to different PEIs at either 4 or 8 μg/mL. Panel (d) represent GSH:GSSG ratio in H1299 and C2C12 cells at 2 h exposure with different PEIs. In c & d, the data were normalized for protein content and are presented as the mean ($n = 4$) ± SD. The columns in (c) & (d) are as follows: 25 k-PEI-B (light grey), 10 k-PEI-B (dark grey) or 25 k-PEI-L (black). Statistical analysis was performed using one-way ANOVA and Tukey's multiple comparisons test (*$p < 0.05$; **$p < 0.01$).

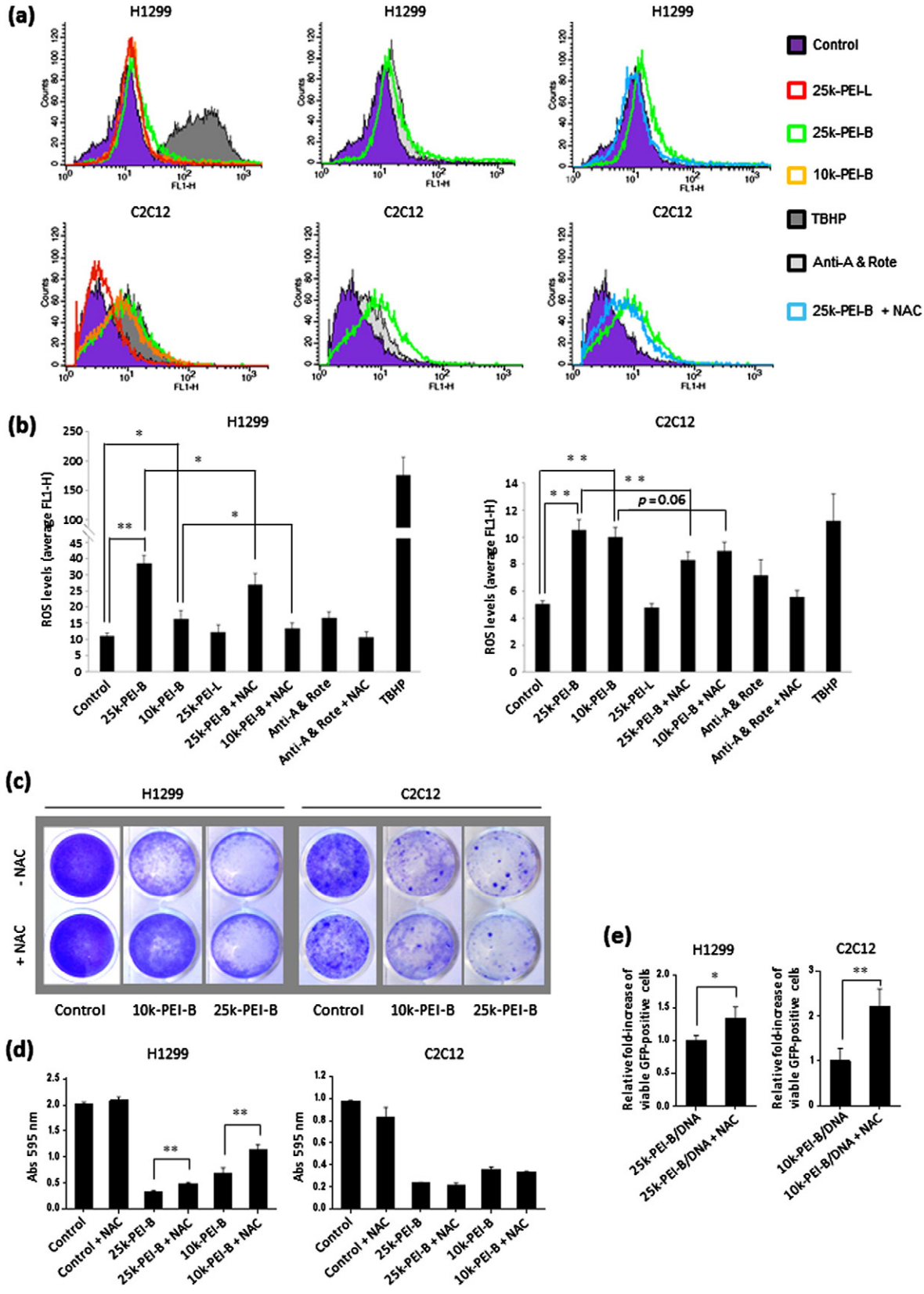

Fig. 7. (a) Representative FACS traces of ROS levels in H1299 and C2C12 cells at 2 h of PEI exposure in the absence and presence of 5 mM *N*-acetyl-cysteine (NAC). PEI concentration was 8 μg/mL. Tert-butyl hydroperoxide (TBHP) or a combination of rotenone (Rote, 2.5 μM) and antimycin-A (Anti-A, 2.5 μM) were used as positive controls for ROS generation. For clarity, different combinations are shown in left, center and right traces. Panel (b) directly compares ROS levels in H1299 and C2C12 from traces in (a). Panel (c) represent photos of adherent H1299 and C2C12 cells following PEI (8 μg/mL) exposure with or without NAC (5 mM), whereas panel (d) is quantification measurement of adherent cells following exposure to branched PEIs (8 μg/mL), with or without 5 mM NAC. Data are shown as the absorbance at λ = 595 nm. Panel (e) shows the viability of H1299 and C2C12 cells expressing GFP on transfection with branched PEI/DNA polyplexes with or without 5 mM NAC. All data are presented as the mean (n = 3) ± SD and statistical analysis was performed with paired students *t*-test to calculate significance (*$p < 0.05$; **$p < 0.01$).

redox homeostasis in two different cell lines, and demonstrated that in addition to an integrated bioenergetic crisis (arising from plasma membrane perturbation and concomitant loss of cytoplasmic glycolytic enzymes/metabolites, and mitochondrial dysfunction), branched PEIs of 10 and 25 kDa, as opposed to a 25 kDa linear counterpart, disturb cellular redox homeostasis through diminished production of NADPH, decreased antioxidant defense capacity of GSH and increased oxidative stress. Indeed, cellular exposure to branched PEIs resulted in rapid acceleration of basal and leak respiration with a transient initial increase of mitochondrial ATP synthesis, whereas linear PEI increased and maintained mitochondrial ATP synthesis over longer periods of time. This demonstrates that on polycation exposure, mitochondria attempt to increase energy production possibly to compensate for energy demanding internalization events [46] and/or energy demanding repair mechanisms [47,48] arising from PEI-mediated insult on plasma membrane and possibly other intracellular structures.

The regulation of mitochondrial energy production is coordinated and multifactorial. Experiments with permeabilized cells and freshly isolated mitochondria demonstrated that PEIs impair OXPHOS in the presence of either CI or CII respiratory substrates. Furthermore, the results from experiments with 'broken mitochondria' demonstrate that all types of PEIs exert a direct inhibitory effect on cytochrome *c* oxidase (CIV). Notably, at low concentrations (0.1–0.5 μg/mL), this inhibitory effect was more profound with 25 kDa branched polycations compared with the linear PEI of same molecular weight. However, at higher PEI concentrations (1–3 μg/mL), the linear PEI approaches and exceeds the inhibitory effect of its branched counterpart, indicating that when the linear architecture has an easy access to the complexes of the ETS (as in the case with 'broken mitochondria') it acts as a potent inhibitor of CIV. Moreover, the extent of PEI architectural- and size-mediated perturbation of mitochondrial energy production and functions was clearly revealed in intact cells. Here, more severe damages (arising from plasma membrane destabilization and impairment of ETS activity) were incurred by the 25k-PEI-B than by the linear counterpart. Even the smaller 10k-PEI-B perturbed plasma membrane and mitochondrial functions more than the 25k-PEI-L on a concentration basis. Accordingly, the branched architectures are superior to the linear geometry in destabilizing mitochondrial membranes (as demonstrated through citrate synthase release from isolated mitochondria) and gaining access to CIV. Therefore, PEI may affect mitochondrial energetic processes either indirectly (through plasma membrane damage and metabolite leakage) and/or directly through perturbation of mitochondrial membranes and potent CIV inhibition. The latter process, perhaps, is more applicable to branched PEIs, but this indicate that polycations should reach mitochondria on cell exposure. Indeed, evidence for this arises from transfection studies with PEI-DNA polyplexes demonstrating that polyplexes (and therefore PEI) can reach mitochondria at early points of transfection [17]. Our observations are therefore relevant to standard transfection protocols involving PEI, since free PEI chains have been suggested to play a critical role in polyplex uptake, transfection efficacy as well as cytotoxicity [49,50]. It is conceivable that macromolecular size and architecture modulate cytoplasmic entry of the polycations (and polyplexes) through diverse sites differently and at different rates, thus influencing their ability to interact with the mitochondrial network. For instance, PEIs of different size and morphology may confer different degrees of detergency activities in destabilizing plasma membrane and/or induce endosome membrane fragment micellization differently. Indeed, branched PEIs may assume globular structures in a similar manner to higher generation polyamidoamine dendrimers [51,52], and induce more effective disruption of biomembranes than a presumed cylindrical geometry of linear PEI. Likewise, PEIs of different geometry may diffuse differently in the gel-like cytoplasm. Indeed, a spherical/globular shape may confer faster diffusion rates (and higher probability on interacting with the mitochondrial network) than a cylindrical morphology.

On PEI exposure, the glycolytic flux was found to rapidly increase in cells. This was presumably to compensate for mitochondrial injury exerted by the polycations and to re-establish bioenergetic homeostasis. Interestingly, with increasing polycation concentrations, branched PEIs not only caused collapse of glycolytic activity, but also reduced intracellular ATP levels. On the contrary, the linear polycation neither impaired the rate of glycolysis nor affected intracellular ATP levels to the same extent as branched PEIs (and notably 25k-PEI-B). Accordingly, branched PEI-mediated collapse of glycolytic activity may partially arise from gradual LDH loss and/or ATP leakage. Indeed, LDH is essential for glycolytic activity and since the initial phase of glycolysis is energy demanding, rapid ATP depletion may further contribute towards impairing the rate of glycolysis. Our results collectively indicate that in contrast to the branched polycationic macromolecules, cells are able to increase both mitochondrial and glycolytic ATP production on exposure to the linear PEI, thus allowing them to respond to increased energy demand following the initial internalization/perturbation events. Conceivably, the linear PEI is less likely to cause serious bioenergetic crisis and overall cessation of energy demanding cellular functions such as the maintenance of ion gradients by Na^+/K^+-ATPase and Ca^{2+}-ATPase. Our observations are also consistent with the extent and the mode of mammalian cell death on exposure to linear or branched PEIs [12], since the extent of ATP fluctuations can trigger cell death either through apoptosis or necrosis [20,26–28].

In addition, to the different extent of bioenergetic crisis observed among the diverse structures of PEIs, the branched molecules perturbed the intracellular redox homeostasis by shifting the balance towards increased oxidative stress. This, presumably, occurs as a result of the combined mitochondrial impairment and glycolytic collapse, resulting in decreased intracellular NADPH levels, which are vital for GSH-mediated antioxidant defense mechanisms [34,35]. Indeed, the GSH:GSSG ratio was decreased following exposure to branched PEIs, indicating accumulation of GSSG, as a result of decreased availability of NADPH and the consequential reduction of NADPH-dependent conversion of GSSG back to GSH. It is likely that PEI (and particularly at higher polycation concentrations)-mediated plasma membrane destabilization, may contribute to intracellular NADPH (and NAD^+) depletion. It is essential for cellular homeostasis to constantly eradicate oxidized and damaged intracellular components, which is usually accomplished by ATP dependent pathways involving proteasomes and lysosomes [47,48]. Interestingly, cellular exposure to branched PEIs resulted in activation of AMPK, a master metabolic regulator, which can be activated in response to various stressors, including ATP deficiency [42] and increased ROS production [53]. AMPK activation can regulate autophagy through its effect on mTOR signaling [54]. Conceivably, our results may offer insights into the autophagy responses previously seen in cells following exposure to branched PEI [16,18]. Co-treatment with the GSH precursor, NAC, significantly increased the numbers of viable cells expressing GFP on transfection with branched PEI-DNA polyplexes. This is indicative of improved cellular antioxidant defense capacity as availability of NAC for GSH synthesis could counteract PEI-mediated rise in ROS levels. These findings clearly demonstrate that in addition to bioenergetic crisis, impairment of redox homeostasis is an important feature of branched PEI mediated cytotoxicity and injury, which is presumably linked to the extent of plasma membrane damage. On the other hand, the reported superior transfection efficiencies of the 25 k-PEI-L may reflect increased cellular survival rates, not only due to its less detrimental effect on biomembranes, but also on cellular bioenergetics and redox homeostasis as shown in this study.

In summary, we have shown that metabolic profiling can improve our mechanistic understanding of polycation-mediated dynamic cell injury at the molecular level. Accordingly, future approaches pertaining design and selection of improved and safer libraries of polycationic vectors may benefit by focusing on integrated biomembrane, chemical and metabolomics combinatorial throughput approaches. Finally, such findings may be translated to engineering of a wide range of

polycationic reagents for manipulation and better understanding of mitochondrial energetics as well as for broader mitochondrial therapeutic interventions applicable to degenerative and metabolic diseases, cancer and aging [55].

Acknowledgements

Financial support by the Danish Agency for Science, Technology and Innovation (Det Frie Forskningsråd for Teknologi og Produktion, reference 274-08-0534 and Det Strategiske Forskningsråd, reference 09-065746/DSF) is gratefully acknowledged. We thank Professor Ernst Wagner (Munich Center for System-based Drug Research, Center for Nanoscience, Ludwig-Maximilians-Universitat, Munich, Germany) for the gift of purified 22 kDa linear PEI.

A.H. and S.M.M. conceived the idea and A.H. wrote the first draft of the manuscript. A.H., M.S. and P.B.J. planned and conducted experiments using Seahorse XF analyzer. A.H. and K.D.M. performed ATP measurements and cellular quantification assays. M.K.L. performed immunoblot analysis. A.H. performed enzyme activity assays. C.C., L.P. and M.R. investigated ROS levels. L.P. and H.A. made polyplexes and investigated transfection efficiency. A.H. made mitochondrial isolations and performed high-resolution respirometry on 'broken mitochondria'. The final manuscript was written by A.H. and S.M.M. with comments from all authors. All authors participated in the interpretation and discussion of the data. The authors declare no competing financial interests.

Appendix A. Supplementary data

Supplementary data to this article can be found online at http://dx.doi.org/10.1016/j.bbabio.2014.12.002.

References

[1] O. Boussif, F. Lezoualc'h, M.A. Zanta, M.D. Mergny, D. Scherman, B. Demeneix, J.P. Behr, A versatile vector for gene and oligonucleotide transfer into cells in culture and in-vivo — polyethylenimine, Proc. Natl. Acad. Sci. U. S. A. 92 (1995) 7297–7301.
[2] A.C. Hunter, S.M. Moghimi, Cationic carriers of genetic material and cell death: a mitochondrial tale, Biochim. Biophys. Acta Bioenerg. 1797 (2010) 1203–1209.
[3] L. Parhamifar, A.K. Larsen, A.C. Hunter, T.L. Andresen, S.M. Moghimi, Polycation cytotoxicity: a delicate matter for nucleic acid therapy-focus on polyethylenimine, Soft Matter 6 (2010) 4001–4009.
[4] S. Patnaik, K.C. Gupta, Novel polyethylenimine-derived nanoparticles for in vivo gene delivery, Expert Opin. Drug Deliv. 10 (2013) 215–228.
[5] E. Wagner, Polymers for siRNA Delivery: inspired by viruses to be targeted, dynamic, and precise, Acc. Chem. Res. 45 (2012) 1005–1013.
[6] M. Zheng, D. Librizzi, A. Kılıç, Y. Liu, H. Renz, O.M. Merkel, T. Kissel, Enhancing in vivo circulation and siRNA delivery with biodegradable polyethylenimine-graft-polycaprolactone-block-poly(ethylene glycol) copolymers, Biomaterials 33 (2012) 6551–6558.
[7] S. Hobel, A. Aigner, Polyethylenimines for siRNA and miRNA delivery in vivo, Wiley Interdiscip. Rev. Nanomed. Nanobiotechnol. 5 (2013) 484–501.
[8] E. Sadeqzadeh, R. Rahbarizadeh, D. Ahmadvand, M.J. Rasaee, L. Parhamifar, S.M. Moghimi, Combined MUC1-specific nanobody-tagged PEG-polysthylenimine polyplex targeting and transcriptional targeting of tBid transgene for directed killing of MUC1 over-expressing tumour cells, J. Control. Rel. 156 (2004) 85–91.
[9] T. Bieber, W. Meissner, S. Kostin, A. Niemann, H.P. Elsasser, Intracellular route and transcriptional competence of polyethylenimine–DNA complexes, J. Control. Release 82 (2002) 441–454.
[10] W.T. Godbey, K.K. Wu, A.G. Mikos, Size matters: molecular weight affects the efficiency of poly(ethylenimine) as a gene delivery vehicle, J. Biomed. Mater. Res. 45 (1999) 268–275.
[11] A.C. Hunter, Molecular hurdles in polyfectin design and mechanistic background to polycation induced cytotoxicity, Adv. Drug Deliv. Rev. 58 (2006) 1523–1531.
[12] S.M. Moghimi, P. Symonds, J.C. Murray, A.C. Hunter, G. Debska, A. Szewczyk, A two-stage poly(ethylenimine)-mediated cytotoxicity: implications for gene transfer/therapy, Mol. Ther. 11 (2005) 990–995.
[13] S. Ferrari, E. Moro, A. Pettenazzo, J.P. Behr, F. Zacchello, M. Scarpa, ExGen 500 is an efficient vector for gene delivery to lung epithelial cells in vitro and in vivo, Gene Ther. 4 (1997) 1100–1106.
[14] J.W. Wiseman, C.A. Goddard, D. McLelland, W.H. Colledge, A comparison of linear and branched polyethylenimine (PEI) with DCChol/DOPE liposomes for gene delivery to epithelial cells in vitro and in vivo, Gene Ther. 10 (2003) 1654–1662.
[15] L. Wightman, R. Kircheis, V. Rössler, S. Carotta, R. Ruzicka, M. Kursa, E. Wagner, Different behavior of branched and linear polyethylenimine for gene delivery in vitro and in vivo, J. Gene Med. 3 (2001) 362–372.
[16] X.L. Gao, L. Yao, Q.X. Song, L. Zhu, Z. Xia, H.M. Xia, X.G. Jiang, J. Chen, H.Z. Chen, The association of autophagy with polyethylenimine-induced cytotoxicity in nephritic and hepatic cell lines, Biomaterials 32 (2011) 8613–8625.
[17] G. Grandinetti, N.P. Ingle, T.M. Reineke, Interaction of poly(ethylenimine)–DNA polyplexes with mitochondria: implications for a mechanism of cytotoxicity, Mol. Pharm. 8 (2011) 1709–1719.
[18] C.W. Lin, M.S. Jan, J.H.S. Kuo, L.J. Hsu, Y.S. Lin, Protective role of autophagy in branched polyethylenimine (25 K)- and poly(L-lysine) (30–70 K)-induced cell death, Eur. J. Pharm. Sci. 47 (2012) 865–874.
[19] P. Symonds, J.C. Murray, A.C. Hunter, G. Debska, A. Szewczyk, S.M. Moghimi, Low and high molecular weight poly(L-lysine)s/poly(L-lysine)–DNA complexes initiate mitochondrial-mediated apoptosis differently, FEBS Lett. 579 (2005) 6191–6198.
[20] A. Hall, A.K. Larsen, L. Parhamifar, K.D. Meyle, L.P. Wu, S.M. Moghimi, High resolution respirometry analysis of polyethylenimine-mediated mitochondrial energy crisis and cellular stress: mitochondrial proton leak and inhibition of the electron transport system, Biochim. Biophys. Acta Bioenerg. 1827 (2013) 1213–1225.
[21] G.T. Babcock, M. Wikstrom, Oxygen activation and the conservation of energy in cell respiration, Nature 356 (1992) 301–309.
[22] Y. Hatefi, The mitochondrial electron-transport and oxidative-phosphorylation system, Annu. Rev. Biochem. 54 (1985) 1015–1069.
[23] P. Mitchell, Chemiosmotic coupling in oxidative and photosynthetic phosphorylation, Biochim. Biophys. Acta Bioenerg. 1807 (2011) 1507–1538.
[24] D. Pesta, E. Gnaiger, High-resolution respirometry: OXPHOS protocols for human cells and permeabilized fibers from small biopsies of human muscle, Methods Mol. Biol. 810 (2012) 25–58.
[25] H. Itoh, A. Takahashi, K. Adachi, H. Noji, R. Yasuda, M. Yoshida, K. Kinosita, Mechanically driven ATP synthesis by F-1-ATPase, Nature 427 (2004) 465–468.
[26] D.S. Izyumov, A.V. Avetisyan, O.Y. Pletjushkina, D.V. Sakharov, K.W. Wirtz, B.V. Chernyak, V.P. Skulachev, "Wages of Fear": transient threefold decrease in intracellular ATP level imposes apoptosis, Biochim. Biophys. Acta Bioenerg. 1658 (2004) 141–147.
[27] W. Lieberthal, S.A. Menza, J.S. Levine, Graded ATP depletion can cause necrosis or apoptosis of cultured mouse proximal tubular cells, Am. J. Physiol. Renal Physiol. 274 (1998) F315–F327.
[28] W.X. Zong, C.B. Thompson, Necrotic death as a cell fate, Genes Dev. 20 (2006) 1–15.
[29] J. Zheng, Energy metabolism of cancer: glycolysis versus oxidative phosphorylation (Review), Oncol. Lett. 4 (2012) 1151–1157.
[30] M.P. Murphy, How mitochondria produce reactive oxygen species, Biochem. J. 417 (2009) 1–13.
[31] T. Finkel, N.J. Holbrook, Oxidants, oxidative stress and the biology of ageing, Nature 408 (2000) 239–247.
[32] B. Halliwell, Oxidative stress and cancer: have we moved forward? Biochem. J. 401 (2007) 1–11.
[33] D. Trachootham, J. Alexandre, P. Huang, Targeting cancer cells by ROS-mediated mechanisms: a radical therapeutic approach? Nat. Rev. Drug Discov. 8 (2009) 579–591.
[34] S.C. Lu, Glutathione synthesis, Biochim. Biophys. Acta Gen. Subj. 1830 (2013) 3143–3153.
[35] S.C. Lu, Regulation of hepatic glutathione synthesis: current concepts and controversies, FASEB J. 13 (1999) 1169–1183.
[36] M.B. Dworkin, E. Dworkinrastl, Regulation of carbon flux from amino-acids into sugar phosphates in xenopus embryos, Dev. Biol. 138 (1990) 177–187.
[37] S.H. Jo, M.K. Son, H.J. Koh, S.M. Lee, I.H. Song, Y.O. Kim, Y.S. Lee, K.S. Jeong, W.B. Kim, J.W. Park, B.J. Song, T.L. Huhe, Control of mitochondrial redox balance and cellular defense against oxidative damage by mitochondrial NADP(+)-dependent isocitrate dehydrogenase, J. Biol. Chem. 276 (2001) 16168–16176.
[38] R.L. Veech, L.V. Egglesto, H.A. Krebs, Redox state of free nicotinamide-adenine dinucleotide phosphate in cytoplasm of rat liver, Biochem. J. 115 (1969) 609–619.
[39] A. Hall, K.D. Meyle, M.K. Lange, M. Klima, M. Sanderhoff, C. Dahl, C. Abildgaard, K. Thorup, S.M. Moghimi, P.B. Jensen, J. Bartek, P. Guldberg, C. Christensen, Dysfunctional oxidative phosphorylation makes malignant melanoma cells addicted to glycolysis driven by the (V600E)BRAF oncogene, Oncotarget 4 (2013) 584–599.
[40] M.D. Brand, D.G. Nicholls, Assessing mitochondrial dysfunction in cells, Biochem. J. 435 (2011) 297–312.
[41] D.G. Nicholls, V.M. Darley-Usmar, M. Wu, P.B. Jensen, G.W. Rogers, D.A. Ferrick, Bioenergetic profile experiment using C2C12 myoblast cells, J. Vis. Exp. (2010), http://dx.doi.org/10.3791/2511.
[42] J.S. Oakhill, Z.P. Chen, J.W. Scott, R. Steel, L.A. Castelli, N. Ling, S.L. Macaulay, B.E. Kemp, beta-Subunit myristoylation is the gatekeeper for initiating metabolic stress sensing by AMP-activated protein kinase (AMPK), Proc. Natl. Acad. Sci. U. S. A. 107 (2010) 19237–19241.
[43] M.X. Tang, F.C. Szoka, The influence of polymer structure on the interactions of cationic polymers with DNA and morphology of the resulting complexes, Gene Ther. 4 (1997) 823–832.
[44] M.X. Tang, C.T. Redemann, F.C. Szoka, In vitro gene delivery by degraded polyamidoamine dendrimers, Bioconjug. Chem. 7 (1996) 703–714.
[45] S. Boeckle, K. von Gerddorff, S. van der Piepen, C. Culmsee, E. Wagner, M. Ogris, Purification of polyethylenimine polyplexes highlights the role of free polycations in gene transfer, J. Gene Med. 6 (2004) 1102–1111.
[46] J. Lu, M. Liong, S. Sherman, T. Xia, M. Kovochich, A.E. Nel, J.I. Zink, F. Tamanoi, Mesoporous silica nanoparticles for cancer therapy: energy-dependent cellular uptake and delivery of paclitaxel to cancer cells, Nanobiotechnology 3 (2007) 89–95.

[47] A. Mani, E.P. Gelmann, The ubiquitin–proteasome pathway and its role in cancer, J. Clin. Oncol. 23 (2005) 4776–4789.
[48] P.J. Plomp, P.B. Gordon, A.J. Meijer, H. Hoyvik, P.O. Seglen, Energy dependence of different steps in the autophagic-lysosomal pathway, J. Biol. Chem. 264 (1989) 6699–6704.
[49] Y. Yue, F. Jin, R. Deng, J. Cai, Y. Chen, M. Lin, K. Hsiang-Fu, C. Wu, Revisit complexation between DNA and polyethylenimine—effect of uncomplexed chains free in the solution mixture on gene transfection, J. Control. Release 155 (2011) 67–76.
[50] Z. Dai, T. Gjetting, M.A. Mattebjerg, C. Wu, T.L. Andresen, Elucidating the interplay between DNA-condensing and free polycations in gene transfection through a mechanistic study of linear and branched PEI, Biomaterials 32 (2011) 8626–8634.
[51] U. Gupta, H.B. Agashe, A. Asthana, N.K. Jain, A review of in vitro–in vivo investigations on dendrimers: the novel nanoscopic drug carriers, Nanomedicine 2 (2006) 66–73.
[52] S. Hong, P.R. Leroueil, E.K. Janus, J.L. Peters, M.M. Kober, M.T. Islam, B.G. Orr, J.R. Baker Jr., M.M.B. Holl, Interaction of polycationic polymers with supported lipid bilayers and cells: nanoscale hole formation and enhanced membrane permeability, Bioconjug. Chem. 17 (2006) 728–734.
[53] A. Alexander, S.L. Cai, J. Kim, A. Nanez, M. Sahin, K.H. MacLean, K. Inoki, K.L. Guan, J. Shen, M.D. Person, D. Kusewitt, G.B. Mills, M.B. Kastan, C.L. Walker, ATM signals to TSC2 in the cytoplasm to regulate mTORC1 in response to ROS, Proc. Natl. Acad. Sci. U. S. A. 107 (2010) 4153–4158.
[54] J. Kim, M. Kundu, B. Viollet, K.L. Guan, AMPK and mTOR regulate autophagy through direct phosphorylation of Ulk1, Nat. Cell Biol. 13 (2011) 132–141.
[55] D.C. Wallace, W. Fan, V. Procaccio, Mitochondrial energetics and therapeutics, Annu. Rev. Pathol. 5 (2010) 297–348.